



OPEN ACCESS

EDITED BY

Ligang Zhang,
Central South University, China

REVIEWED BY

Masoud Salavati-Niasari,
University of Kashan, Iran
Khaled Jawad Habib,
Kuwait Institute for Scientific Research,
Kuwait

*CORRESPONDENCE

Liang Song,
moushangliao@163.com

SPECIALTY SECTION

This article was submitted to Structural Materials, a section of the journal Frontiers in Materials

RECEIVED 31 May 2022

ACCEPTED 05 July 2022

PUBLISHED 25 August 2022

CITATION

Song L, Peng Y, Zhao H, Cao Y and Fang Q (2022), Corrosion resistance analysis of the weld metal of low-alloy high-strength steel considering different alloy compositions. *Front. Mater.* 9:957669. doi: 10.3389/fmats.2022.957669

COPYRIGHT

© 2022 Song, Peng, Zhao, Cao and Fang. This is an open-access article distributed under the terms of the [Creative Commons Attribution License \(CC BY\)](https://creativecommons.org/licenses/by/4.0/). The use, distribution or reproduction in other forums is permitted, provided the original author(s) and the copyright owner(s) are credited and that the original publication in this journal is cited, in accordance with accepted academic practice. No use, distribution or reproduction is permitted which does not comply with these terms.

Corrosion resistance analysis of the weld metal of low-alloy high-strength steel considering different alloy compositions

Liang Song^{1,2*}, Yun Peng², Haiyan Zhao¹, Yang Cao² and Qian Fang³

¹Tsinghua University, Beijing, China, ²Central Iron & Steel Research Institute, Beijing, China, ³Hebei University of Technology, Tianjin, China

In order to find the low-alloy high-strength steel welded with the strongest corrosion resistance, the corrosion resistance of HSAL weld metal was studied by considering different alloy compositions. Corrosion resistance of alloy compositions of 460, 690, and 980 MPa was analyzed in an atmospheric environment and simulated seawater environment, respectively. The results of the corrosion weight gain test, weight loss test, and Kelvin probe test showed that the HSAL weld metal with 980 MPa alloy composition has the best corrosion resistance in an atmospheric environment. Through seawater immersion and electrochemical testing, it was found that the HSAL weld metal with 980 MPa alloy composition had good corrosion resistance in a simulated seawater environment, the HSAL with 690 MPa alloy composition had medium corrosion resistance, and the HSAL with 460 MPa alloy composition had the lowest corrosion resistance. The corrosion resistance of the weld zone is the best and that of the heat-affected zone is the worst; these findings may be helpful for research in related fields.

KEYWORDS

HSAL, corrosion resistance, weld metal, atmospheric environment, simulated seawater environment, seawater immersion test, electrochemical test

1 Introduction

The accelerated pace of global economic integration promotes integration of China's steel market with the international market. While introducing high-tech, high-performance, and high-strength steel, China has also made strategic adjustments and improvements in the production process and technology of high-strength steel (Ding et al., 2020). Compared with structures made from ordinary strength steel, structures of high-strength steel have the following advantages: (1) improvement in the steel strength can reduce the thickness of the steel plate, reduce the size of components, and reduce the amount of steel needed, so as to reduce the structure weight and weaken seismic function; (2) high-strength steel can reduce the weld size, decrease the amount of welding materials and welding workload, improve weld quality, and improve the useful life of the structure

(Ogawa and Osuki, 2020); and (3) the reduction of steel and welding material consumption can greatly reduce energy consumption in iron and steel smelting, and the consumption of iron ore resources, which is consistent with the requirements of building a low-carbon society in China. China's steel specifications GB/T8162-2008 "Seamless Steel Tubes for Structures" and GB/T1591-2008 "(High Strength Low Alloy, HSAL) Structural Steels" are listed in Q460, Q500, Q690, and Q980 strength grade high-strength steel, respectively. GB50017-2003, "Code for Design of Steel Structures," is listed in Q420 steel, and other high-strength steel is being studied in the new code (Zhang et al., 2018a; Ma et al., 2018; Garcia and Procópio, 2020; Shen et al., 2020). HSAL is widely used in bridge construction and shipbuilding because of its beneficial mechanical properties and high resistance to fractures.

In order to realize the benefits of high-strength and low-alloy weld metal in more fields, it is necessary to determine its corrosion resistance, which has been studied by some current scholars. For example, Yang et al. found that the content of diffused hydrogen in casting welds was closely related to the carbon content. The higher the carbon content, the lower the diffused hydrogen content. Moreover, the behavior of hydrogen in gray cast iron was similar to that of steel. With the increase of diffusive hydrogen content, critical stress would gradually decrease and the tendency to crack would gradually increase (Yang et al., 2018). Zhang et al. studied the relationship between hydrogen and steel tensile strength and concluded that after hydrogen charging, the notch tensile strength of high-strength steel decreased. With the increase of diffusible hydrogen content in steel, the tensile strength of steel decreased in the power function form. These researchers found that fracture of non-hydrogen-filled samples produced a ductile dimple shape, and the fracture mode was intergranular (Zhang et al., 2018b). Song et al. found in their study of hydrogen diffusion in Q960 steel that the permeation time and diffusion coefficient of hydrogen atoms in steel would be prolonged and reduced due to the hydrogen trap. When there are reversible and irreversible hydrogen traps in the material, the hydrogen diffusion coefficient will be different. Generally, the former is greater than the latter. However, the diffusion coefficient of hydrogen will not change with the thickness of the sample (Song et al., 2019). In addition, in studying the effect of hydrogen on the resistance to the fracture of stainless steel welds, Kw et al. showed that hydrogen would reduce fracture resistance, even if the hydrogen charging time was very short. In addition, hydrogen entering the metal would also affect its microstructure and the loading rate (Wang et al., 2018). Radhamani et al. found that due to the influence of martensite and retained austenite in the metal, the hydrogen content is relatively high in the weld zone and heat-affected zone of steel, which easily leads to brittle fractures at the metal's edge (Radhamani et al., 2020). Gucwa et al. also showed that when the cathodic polarization potential increased from -1,050 mV to -850 mV, the hydrogen embrittlement of low-alloy steel decreased significantly (Gucwa et al., 2019).

Although domestic and foreign scholars have studied some properties of Q460, Q500, Q690, Q980, and other high-strength steels, there are few studies on the cathodic protection properties of high-strength dissimilar steel weldments. Especially for high-strength steel with a yield strength greater than 900 MPa, it is impossible to understand the corrosion resistance of high-strength low-alloy weld metal under different alloy compositions. In order to advance this research and find the low-alloy high-strength steel with the strongest corrosion resistance, we studied the corrosion resistance of 460, 690, and 980 MPa HSAL weld metal in atmospheric environments and simulated marine environments. By analyzing the corrosion resistance of weld metals with different alloy compositions (460, 690, and 980 MPa) in those environments, we are able to provide insight into the corrosion resistance of weld metals of low-alloy steel with different alloy compositions and demonstrate their applicability to more fields.

2 Materials and methods

2.1 Experimental materials

HSALs 460, 690, and 980 MPa were produced by Guangdong Jiahaogang Mould Co., Ltd. Each of the different HSAL compositions were cut into components of equal size. HSALs of the same composition were welded into pairs to obtain HSAL samples of differing composition. NaHSO₃ solution was purchased from Shandong High Strength Steel Plate Sales Co., Ltd; Derusting solution from Suzhou Huamo Environmental Protection Technology Co., Ltd; HCl from Shaanxi Qiyue Biotechnology Co., Ltd; C₆H₁₂N₄ from Hebei Jiashuo Chemical Technology Co., Ltd; ethanol from Shandong Yinrun Chemical Co., Ltd; acetone from Guangdong Yinhe Chemical Co., Ltd; and NaCl solution from Hubei Sentai Materials Co., Ltd.

2.2 Experimental instruments

A JR-A simulated etching testing machine was purchased from trial manufacturing in southern Jiangsu and Versa scan SKP was produced by Princeton Company of the United States. Analytical balance, Current meter, 3D video microscope, scanning electron microscope; Chi660c electrochemical workstation were purchased from Shanghai Chenhua Instrument Co., Ltd.

2.3 Experimental method

2.3.1 Analysis of the corrosion resistance in an atmospheric environment

The primary purpose of the test in this section was to simulate the corrosion resistance of patterns of the HSAL

weld metal with different alloy compositions in an atmospheric environment. The test specimens were prepared as outlined below.

The test adopts the “periodic infiltration accelerated corrosion test”, and the test process refers to the national standard “Immersion Test of Corrosion Salt Solution of Metals and Alloys” (GB/T19746-2005) (Jiang et al., 2019). The test instrument used was a “JR-A simulated etching tester,” manufactured by Sunan environmental test. The HSAL weld metal pattern for each alloy composition has several parallel samples, which were used for corrosion weight gain analysis, weight loss analysis, and probe test analysis, respectively. The cycle of the weekly immersion test was 60 minutes, including 12 minutes for infiltration, and 48 minutes for drying (water bath temperature $(25 \pm 2)^\circ\text{C}$, air temperature $(25 \pm 2)^\circ\text{C}$, relative humidity $(45 \pm 2)\%$ RH). Test periods were 48, 150, 222, 318, and 390 h, respectively. The test solution was 0.01 mol/L NaHSO_3 , and the supplementary solution was 0.02 mol/L NaHSO_3 . The sample size was measured and weighed before each test cycle, and after the test, the samples were tested for corrosion weight loss.

1) Corrosion weight gain test

A weight gain experiment method was used. The HSAL weld metal pattern with three different alloy components was cut into $40 \text{ mm} \times 40 \text{ mm} \times 3\text{-}5 \text{ mm}$ squares (including weld, base metal, and heat affected zone) to mill and polish the iron oxide layer on the surface. The corrosion working surface was $2 \text{ mm} \times 2 \text{ mm}$ (for the weld), the experimental temperature was 30°C , and humidity was 60%. Taking 12 hours as a cycle, 80 cycles were performed to measure corrosion weight gain. Rust layer morphology was observed by sampling in two stages: XRD diffraction phase analysis and electrochemical curve measurement.

2) Scanning Kelvin probe test

Scanning Kelvin probe (SKP) is the first technology used to measure the work function of steel surfaces in the atmosphere. In the early 1990s, SKP vibration capacitance technology was first applied to corrosion-related directions. It was especially widely used in researching of electrochemical reactions on metal surfaces and corrosion between dissimilar steels. This technology can detect the potential distribution on the surface without contacting the sample. It has high resolution and is very sensitive. It can detect the location and makeup of metal corrosion in a single assessment. The system can automatically complete data acquisition and processing during the test. The three-dimensional platform used to place the sample can be adjusted in the x - y - z axis to ensure that the position between the probe and the sample is always consistent.

The SKP test system is modeled on the Versa SCAN SKP, which is produced by the United States' Princeton company. The test is carried out in a room temperature atmospheric environment. Before the test, the x - y - z axis of the three-dimensional platform is adjusted to ensure that the distance between the sample and the probe is always consistent during testing. During the test, the probe used is made of platinum alloy, and the distance between the probe and the sample needs to be adjusted to $100 \mu\text{m}$. The scanning probe test scans from the base metal to the weld area. This scanning type adopts surface scanning, and the scanning area is $75 \text{ mm} \times 15 \text{ mm}$; scanning speed is $200 \mu\text{m/s}$; the moving scanning mode of step length is adopted in the test process, and the step length of the x - and y -axis is $200 \mu\text{m}$. Resolution is $20 \mu\text{m}$. Vibration frequency is 2 kHz, and the test sensitivity is $20 \mu\text{V}$ to ensure that the instrument does not generate overload, and the absolute value adjustment of the test signal should be less than 1 V. For ease of description, the test results are displayed by the two-dimensional effect.

SKP is the third generation of local electrochemical testing technology. It is very effective in detecting local differences on sample surfaces. During the test, the probe does not contact the sample surface, so it will not damage the material surface or properties. This technology can test a variety of materials, such as conductors and semiconductors. The usual test environment is an atmospheric environment. In addition, the test technology can also be applied to gaseous humid environments, which is a scientific and technological breakthrough. In our experiment, the scanning Kelvin probe was used to accurately scan different micro areas of the HSAL weld metal with different alloy compositions. In the scanning process, the probe can obtain the work function of the material surface, so as to distinguish differences in metal surfaces through the work function value. In addition, according to the existing theory, it is found that the voltaic potential difference ($\Delta\Psi$) between the Kelvin probe and the sample is related to the self-compound potential (E_{corr}) of the material:

$$E_{corr} = \Delta\Psi + Const \quad (1)$$

where *Const* is a constant term, and its value can be determined by the test. Therefore, the galvanic corrosion performance of the material can be analyzed by using the difference of the surface voltaic potential of the sample measured by the Kelvin probe.

3) Analysis of the corrosion weight loss test

In the first step, corrosion products on the surface of the test steel were cleaned with derusting solution. The composition of the derusting solution is 500 ml HCl +500 ml distilled water +3.5 g hexamethylene tetramine ($\text{C}_6\text{H}_{12}\text{N}_4$). After rust removal, the test steel was cleaned with deionized water, soaked in ethanol

TABLE 1 Chemical composition of the medium solution.

Chemical name	Composition/%
NaCl	2.4291
KCl	0.0743
MgCl ₂	0.3243
CaCl ₂	0.2111
MgSO ₄	0.3991

solution, then taken out, blown dry, and stored in a dryer. After 24 hours in the dryer, an analytical balance was used to weigh and record the test item's mass after rust removal. Equation 2 is used for the calculation of corrosion weight loss rate W :

$$W = \frac{(G_0 - G_1) \cdot 10^6}{2(a \cdot b + a \cdot c + b \cdot c)t} \quad (2)$$

where G_0 represents the original weight of the pattern, G_1 represents the weight after corrosion, a is the length of the pattern, t is the corrosion time, and b and c represent time width and thickness, respectively.

2.3.2 Analysis of corrosion resistance in seawater environment

Seawater is a natural strong electrolyte, in which Cl⁻ will further destroy the passive film on the metal surface, cause pitting corrosion on the local surface of the structure, and affect the service performance of HSAL. In this paper, we studied the corrosion resistance of weld metal samples of HSAL with different alloy components under the influence of seawater corrosion. The preparation of the experimental solution and the corrosion process are described as follows:

The accelerated corrosion test of indoor simulated seawater is carried out according to the Russian national standard GOST9.911-89. The simulated test is the equivalent of the seawater environment in tidal areas, in which the oxygen concentration is close to saturation, and the chemical composition of the medium solution is as shown in Table 1.

First, for HSAL weld metal samples with different alloy components, the surface of the steel sample was polished successively with various weights of sandpaper (the highest level is 1,200#). Next, the oil was removed with acetone and dehydrated with absolute ethanol, left to dry for a specified period; then the initial quality of the steel sample was weighed. Then, the samples of the HSAL weld metal with different alloy components were vertically placed in the medium solution and soaked at room temperature for 5 days. An ammeter was placed in the system to simulate the current. The medium solution was changed every day to ensure that its concentration remained constant. After soaking, the corrosion products on the surface of the steel sample were removed with a derusting solution (500 ml hydrochloric acid +500 ml deionized water +10 g

hexamethylene tetramine), and the derusted sample was cleaned with absolute ethanol and blown dry. After drying for 24 hours, the sample was weighed, and the corrosion of the derusting solution was corrected to the substrate with the non-corroded sample. Thereafter, the following tests were carried out:

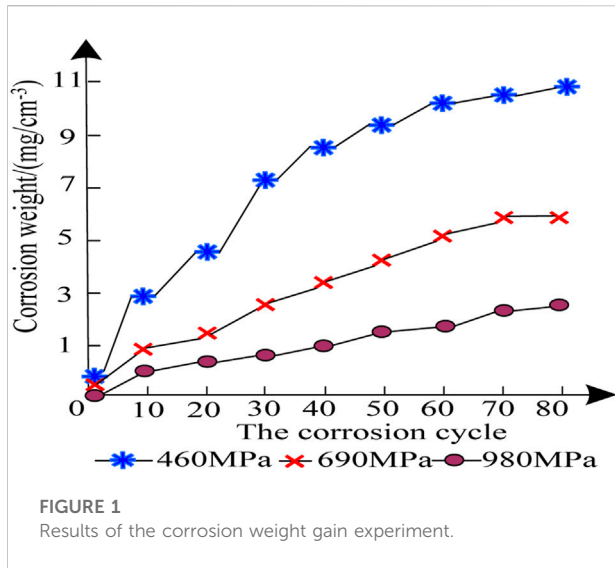
1) Seawater immersion corrosion test

The samples (460, 690 and 980 MPa) of HSAL weld metal with different alloy compositions are polished to 1,500 #, soaked in seawater for 30 days, with the seawater being changed every seven days. At the end of the test, the outer rust layer on the surface is cleaned with distilled water and dried, and then observed with a three-dimensional video microscope (Lanzutti et al., 2019) After that, the corrosion products are removed and pickled (pickling solution: 1,000 ml hydrochloric acid of 1.1 g/cm³ and 20 g hexamethylenetetramine), and the surface corrosion micro-morphology is observed through a scanning electron microscope.

2) Differing seawater concentrations

The corrosion resistance of samples of the HSAL weld metal with different alloy compositions under differing seawater concentrations is simulated by adjusting the concentration of NaCl solution. The concentrations of NaCl solution are 3.5%, 4.5%, 5.5% and 6.5%, respectively. The changes in self-corrosion current of samples of the HSAL weld metal with different alloy components were analyzed. The corrosion resistance of the sample was analyzed by the electrochemical test.

The electrochemical test was carried out according to the corrosion standard CTO00190242-001-2008 "Method for Determining the Local Corrosion Stability of Carbon Steel and Low Alloy Steel," formulated by the Russian Central ferrous Metallurgy Research Institute. This method was used to evaluate local corrosion resistance in a water environment containing Cl⁻. The electrochemical test was carried out on a CHI660C electrochemical workstation (Shanghai Chenhua Instrument Co., Ltd.), using a 3-electrode system (HSAL weld metal samples with different alloy compositions as a working electrode, Pt sheet as an auxiliary electrode, and saturated Ag/AgCl as a reference electrode). By recording the potentiodynamic polarization curves of the samples in the positive and negative directions, parameters are determined that can evaluate the corrosion performance of samples of the HSAL weld metal with different alloy components, including: corrosion potential $E_i = 0$, current density $i_E = -300$ mV when the potential is -300 mV (saturated silver chloride electrode), potential E_{corr} with the maximum current density i_{max} . The



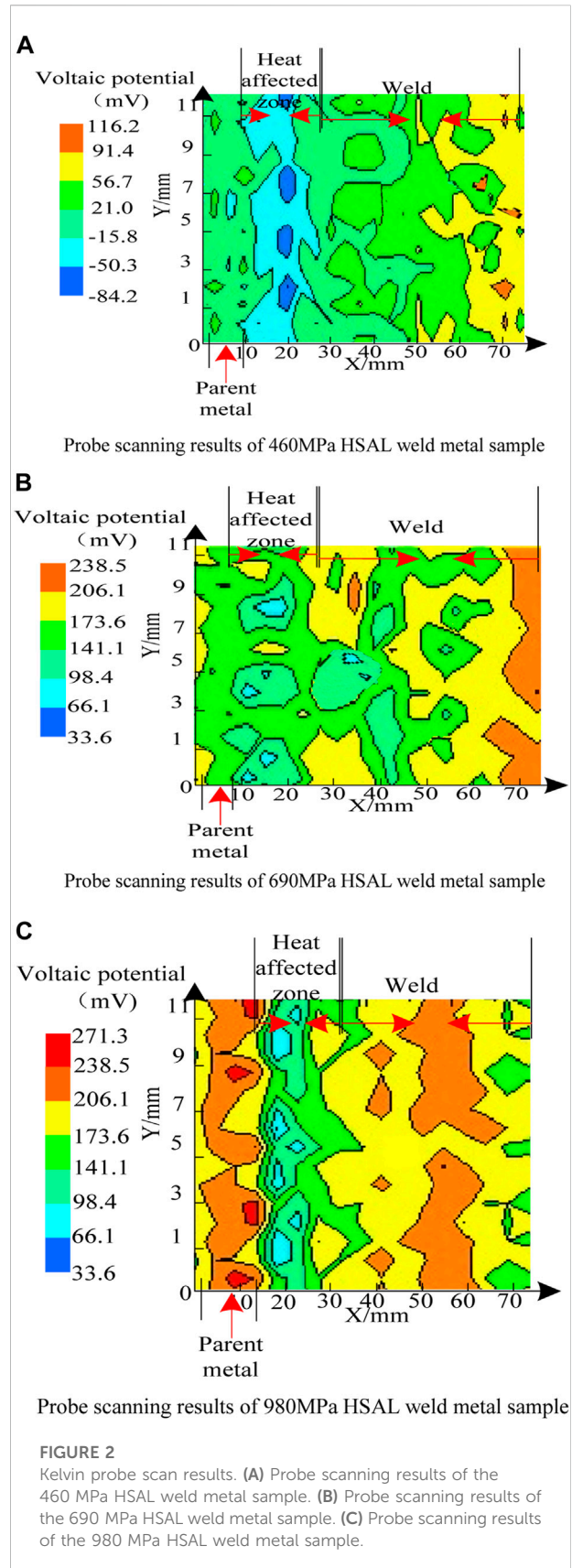
corrosion resistance of the sample is judged by the change in the self-corrosion current.

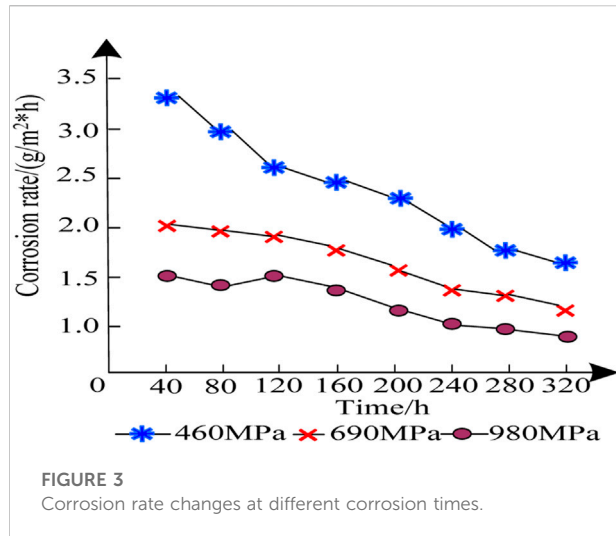
3 Results

3.1 Results of the corrosion weight gain test

The corrosion weight gain results of patterns of the HSAL weld metal with three different alloy compositions are shown in Figure 1.

It can be seen from Figure 1 that in the early stage of corrosion, the corrosion weight gain rate of the weld metal patterns of three kinds of HSAL with three different alloy compositions is large, and the corrosion weight gain shown on the curve is not different. After 10 corrosion test cycles, the corrosion weight gain rate of the 460 MPa HSAL weld metal pattern was faster than that of the 690 MPa HSAL and 980 MPa HSAL weld metal patterns, and the gap between them gradually increased. After 40 cycles, the corrosion weight gain of the 690 MPa HSAL and 980 MPa HSAL weld metal patterns were slow, and the corrosion rate decreased, while the corrosion weight gain rate of the 460 MPa HSAL weld metal pattern began to decrease around 60 cycles. As shown by the above test results, it can be seen that the corrosion weight gain of the 690 MPa HSAL and 980 MPa HSAL weld metal patterns was relatively close, but the corrosion weight gain of the 690 MPa HSAL weld metal pattern was higher. The corrosion weight gain of the 4600 MPa HSAL weld metal pattern was the largest; that is, the corrosion condition of this pattern was the most serious.





This may be caused by the different tensile strength of the HSAL weld metal. The stronger the tensile strength, the stronger the corrosion resistance. On the contrary, if the tensile strength is weak, corrosion occurs easily.

3.2 Experimental results of SKP

The two-dimensional plane scanning results of the HSAL weld metal with different alloy components by SKP are shown in Figure 2.

As seen in Figure 2, the micro-zone voltaic potential of HSAL weld metal samples was quite different. The voltaic potential in the base metal area of the 460 MPa HSAL weld metal sample was about 21–56 mV, while the voltaic potential in the heat-affected zone of the sample was significantly negative, with the most negative value being about –84 to –50 mV near the fusion line, indicating that the electron escape work in the heat-affected zone decreased, and it was easier to lose electrons, possibly due to the heat input in the fusion zone. It was caused by the precipitation of carbides and the increase of lattice defects. From the heat-affected zone to the weld zone, the voltaic potential difference gradually increased to about 91 mV, which indicates that the surface of the weld zone was more stable and the difficulty of electron escape increased, which is related to the ferrite structure of the sample weld zone. The potential of the heat-affected zone of the 690 MPa HSAL weld metal sample was about 66–98 mV, and the potential of the base metal zone was about 173 mV, significantly higher than that of the 460 MPa HSAL weld metal sample. The voltaic potential in the base metal area of the 980 MPa HSAL weld metal sample was about 173–271 mV, and the voltaic potential in the heat-affected zone decreased significantly, and the lowest value was about 60 mV (near the fusion line), indicating that it is easy to lose

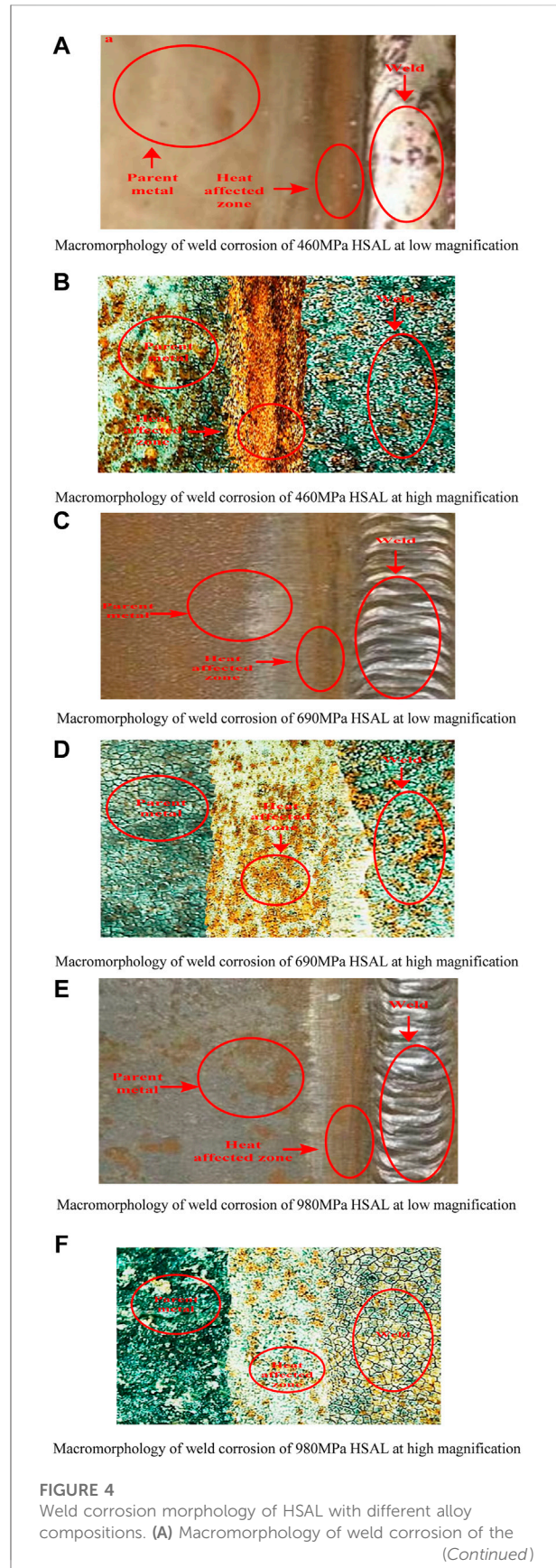


FIGURE 4

460 MPa HSAL at low magnification. (B) Macromorphology of weld corrosion of 460 MPa HSAL at high magnification. (C) Macromorphology of weld corrosion of 690 MPa HSAL at low magnification. (D) Macromorphology of weld corrosion of the 690 MPa HSAL at high magnification. (E) Macromorphology of weld corrosion of 980 MPa HSAL at low magnification. (F) Macromorphology of weld corrosion of 980 MPa HSAL at high magnification.

electrons, which may be related to the serious structural defects caused by heat input. The voltaic potential in the weld area was about 173–238 mV, but it fluctuated greatly due to welding and external reasons. The SKP test results show that the 980 MPa HSAL weld metal sample had the best corrosion resistance, and the V A potential of this sample was the highest, especially at the weld, which was significantly higher than the other two samples. The dense martensite in this region reduced the electron escape rate and improved corrosion resistance. The corrosion resistance of the 460 MPa HSAL weld metal sample was lowest, and the potential of the heat-affected zone near the weld was the lowest, making it more prone to corrosion.

3.3 Results of the corrosion weight loss rate test

The corrosion rate of the two samples under different corrosion times is calculated by Equation 2; the results are presented in Figure 3.

As seen in Figure 3, the corrosion rates of the three groups of patterns show a downward trend with the extension of time, and the corrosion rate of the 980 MPa HSAL weld metal sample is clearly lower. With the extension of the test time, the corrosion rate of the 980 MPa HSAL weld metal sample was significantly lower than those of the 460 MPa HSAL and 690 MPa HSAL weld metal samples. The corrosion rate of the 980 MPa HSAL weld metal sample slightly decreased with the extension of the corrosion test time. The corrosion resistance of the 980 MPa HSAL weld metal sample was definitively better than those of the 460 MPa HSAL and 690 MPa HSAL weld metal samples, and the effect of atmospheric corrosion resistance was also better. The explanation for this lies with the tensile strength, that is, high tensile strength can significantly reduce the corrosion rate of high-strength aluminum alloy weld metal.

3.4 Results of full immersion seawater corrosion test

According to the SKP test described above, each micro-zone of the HSAL weld with different alloy compositions has different voltaic potential, and the portion near the fusion

line in the heat-affected zone, which may be the most corrosion-resistant area, has the lowest. However, in order to compare with the actual corrosion of the weld, it was necessary to conduct a full immersion corrosion test on the material. Figure 4 shows the corrosion morphology under low and high power mirrors.

Figures 4A,C,E show the macro morphology of weld corrosion of 460, 690, and 980 MPa HSAL welds under low- and high-power microscopy. Figures 4B,D,F show the macro morphology of weld corrosion of 460, 690, and 980 MPa HSAL welds under low-power microscopy. Uneven corrosion products were distributed on the weld surface of HSAL welds. Among them, the 460 MPa HSAL weld was seriously corroded. There was a yellow rust layer in this area, showing comprehensive and uniform corrosion characteristics. After corrosion, the weld surface was covered with a large number of uneven corrosion products, and the yellow rust layer was obvious. The whole shows the characteristics of uniform corrosion; the spot corrosion morphology of the 690 MPa HSAL weld was the same as that of the 980 MPa HSAL weld. The corrosion morphology of the 690 MPa HSAL weld was slightly better than that of the 460 MPa HSAL weld but still worse than that of the 980 MPa HSAL weld. The corrosion, mainly pitting, began in a location conducive to corrosion. Corrosion gradually spread, with the weld corrosion of the 980 MPa HSAL being the smallest. Figure 4, summarizing the analysis of the overall surface of each sample, shows that corrosion in the heat-affected zone between the weld and the base metal was the most serious, especially in the heat-affected zone of the 460 MPa HSAL weld. The surface corrosion area of the base metal was relatively large, producing dense holes, some holes deep. Corrosion products in the base metal area were well-compacted. The yellow rust layer was not obvious, so corrosion resistance was comparatively best. There were many, uneven corrosion byproducts in the base metal area of the 690 MPa HSAL weld; corrosion was noticeably greater than that of the weld. The HSAL weld can form a multi-electrode system in the solution, which can form an extremely complex electrochemical cell in the electrolyte. For the electrode reaction in any area, if equilibrium potential is higher than mixed potential in the solution, the cathode reaction will be carried out; otherwise, the anode reaction will be carried out. This situation is caused mainly by the relatively dense bainite in the weld of 690 MPa HSAL. The test results indicate that the base metal area and weld area of 9 MPa HSAL will be the anode in the primary cell. However, compared with the heat-affected zone, they will be the cathode in the corresponding primary cell. The surface corrosion area of the base metal area was small, characterized by shallow and connected corrosion pits, and a small degree of corrosion. This was affected by the abundance of martensite in the weld. The base metal and weld area of 690 MPa HSAL not only accelerated the galvanic corrosion in the base metal area, but also promoted the corrosion in the heat-affected area. The corrosion degree in the weld area was lower than that of

TABLE 2 Anodic polarization changes of samples in simulated seawater at different concentrations.

NaCl content/%	Sample (Mpa)	E_{corr}/V	I_{corr}/A	R/Ω
3.50	460	-0.9989	2.893×10^{-5}	1,532
	690	-1.0122	9.879×10^{-6}	2,641
	980	-0.9989	3.372×10^{-6}	2,762
4.50	460	-1.0159	3.148×10^{-5}	1,486
	690	-1.0178	1.336×10^{-5}	2,232
	980	-1.0031	2.998×10^{-6}	2,385
5.50	460	-1.0138	2.400×10^{-5}	1,838
	690	-0.9860	2.228×10^{-5}	11,427
	980	-0.9954	7.181×10^{-6}	3,489
6.5	460	-0.9999	3.254×10^{-5}	1,427
	690	-1.0211	1.577×10^{-5}	2,411
	980	-0.9681	7.245×10^{-7}	1,915

the base metal area. There were many dense surface holes, but the depth and pitting were smaller than that of the base metal. Although the number of corrosion pits in the heat-affected zone was small, the pitting area was the largest, and there were some pitting pits. The welded alloy high-strength steel formed multiple galvanic corrosion galvanic cells in seawater. The heat-affected zone was used as the transition area between the weld and the base metal, and as the anode in the galvanic cell, which is the area of quickest and most serious corrosion. As Figure 4 illustrates, under seawater corrosion, the 980 MPa HSAL weld had the highest corrosion resistance, followed by the 690 MPa HSAL weld, and the 460 MPa HSAL weld had the weakest corrosion resistance.

3.5 Results of the analysis of corrosion under different seawater concentrations

The changes in anodic polarization of samples of HSAL weld metal with different alloy compositions under different simulated seawater concentrations are shown in Table 2.

Table 2 details the order of self-corrosion current in 3.5% NaCl, 4.5% NaCl, 5.5% NaCl, and 6.5% NaCl simulated seawater solution: 460 MPa HSAL weld metal sample >690 MPa HSAL weld metal sample >980 MPa HSAL weld metal sample. Since the smaller the self-corrosion current, the better the corrosion resistance is, the corrosion resistance of the 460 MPa HSAL weld metal sample was poor. The reason for this is that when martensite was combined with the 980 MPa HSAL weld metal sample, it improved the stability of the martensite, ensured that martensite was fine and uniform, formed on the surface of the 980 MPa HSAL weld metal sample as an as-cast structure, and protected the 980 MPa HSAL weld metal sample from seawater corrosion. The 690 MPa HSAL weld metal sample was composed

mainly of bainite, a relatively uniform structure. After welding with the welding wire material, the weld structure was relatively uniform, the principle was a high point, there was slight galvanic corrosion, and corrosion resistance was relatively moderate. The 460 MPa HSAL weld metal sample was mainly ferrite. As a consequence, the manganese element formed large austenite on the weld surface during welding, and formed a coarse Widmanstatten structure on the weld surface after cooling, with poor corrosion resistance. It is the above differences that lead to the corrosion resistance of 980 MPa HTS weld metal sample > 690 MPa HTS weld metal sample > 460 MPa HTS weld metal.

4 Discussion

During the corrosion resistance analysis of the HSAL weld metal, corrosion of welded joints was most serious of the entire component. Therefore, in-depth study of corrosion resistance of welded joints would be of great significance for the safe use and life assessment of HSAL components. In addition, because 460 MPa HSAL weld metal is ferritic stainless steel, it contains little or no nickel, and its raw material cost is low. Ferritic stainless steel has a low coefficient of thermal expansion and good resistance to pitting corrosion and high-temperature oxidation. Ferritic stainless steel has the advantages of light weight, stable performance, strong atmospheric corrosion resistance, with good formability and weldability. These properties can well serve the requirements of automotive steel. Therefore, from the perspective of environmental protection and energy conservation, 460 MPa HSAL is widely used in automotive exhaust systems (Sinhar and Dwivedi, 2018). As for 690 MPa HSAL weld metal, it is the most typical bainitic steel with corrosion resistance, heat resistance, high and low temperature strength, good mechanical properties, deep drawing, bending and other room temperature processing properties. It can be widely used in medical devices, auto parts, building materials, and the food, chemical, agriculture, and other industries. The 980 MPa HSAL weld metal has the advantages of high strength, relatively light weight, less energy absorption than other metals, good safety, and processing performance, high strength and corrosion resistance, and can be widely used in bridges and high-rise buildings.

Weldability refers to the characteristics that the same or dissimilar metal material forms with a welded joint with certain service performance under welding conditions. Weldability is affected by the type of material, welding method, component type, and service requirements. Weldability has two meanings: the first is process weldability, which is the sensitivity of some metals to welding defects under specific welding processes (Sarkar et al., 2018). The second, service performance (also known as service weldability), is the extent to which the welded joint formed by metal materials under specific welding

conditions is suitable for service conditions. Since most low-alloy high-strength steel needs to be welded during use, welding quality directly affects the properties of HSAL steel (Zhang et al., 2019). The weld joint of HSAL consists of a weld zone, heat-affected zone, and base metal (base metal) zone (Tomarov et al., 2019). The corrosion resistance of HSAL weld metal with different alloy compositions is closely related to its microstructure.

The microstructure of the HSAL weld metal zone with different alloy compositions is a uniform, mainly single-phase structure, and rarely subject to galvanic corrosion. In the atmospheric environment corrosion simulation test, the structure of heat affected zone was coarse and uneven, including ferrite and austenite (460 MPa HSAL weld metal) or bainite and austenite (690 MPa HSAL weld metal), martensite and austenite (980 MPa HSAL weld metal), which is prone to serious galvanic corrosion. The base metal zone was affected by different levels of heat, and structure size was also different, but it was smaller than the heat-affected zone, and the galvanic corrosion was lighter. The corrosion of HSAL weld metal was determined by corrosion weight gain analysis, probe analysis, and medium corrosion analysis. The corrosion resistance of weld metal at 460 MPa is significantly lower than that at 690 and 980 MPa. The degree of corrosion of the three areas of the HSAL weld metal is heat affected area > base metal area > weld area. During the test, the corrosion resistance of the HSAL weld metal with different alloy compositions in seawater was simulated. Analysis results found that the 460 mPa HSAL weld metal had obvious corrosion, and the corrosion was most serious under differing seawater concentrations. The 980 mPa HSAL had the best corrosion resistance. Under a simulated seawater environment, the degree of corrosion of the weld metal zone of three alloy steels was basically the same: heat affected zone > base metal zone > weld metal zone.

In the study of the corrosion resistance of welded structures, the study of the corrosion resistance of welds is not enough. This is mainly because of the electrochemical corrosion characteristics of the weld area and the inhomogeneity of the weld. The corrosion behavior of the welded joint of pipeline steel may be different from that of the base metal, especially the welding residual stress closely related to the welding process. Therefore, the earliest work in this area was research on welding residual stress, mainly studying post-weld heat treatment and adjusting the welding process, so as to reduce welding residual stress and improve the corrosion resistance of the welded structure (Kse, 2020). After determining the corrosion system and corrosion environment of the base metal, the alloy composition and the content of the welding material are important factors that determine the composition, structure, and performance of the weld. However,

the influence mechanism of alloy elements on the corrosion properties of weld metals is still not well understood. In addition, the corrosion resistance of the material changes greatly under different working conditions. The specific environmental medium conditions must be considered when adjusting the weld composition. Therefore, when selecting welding materials, it can only be determined through tests according to the specific corrosion system, in order to select appropriate welding materials to ensure that the welded joints are excellent and free of defects. When selecting welding materials, according to the weldability of the weld, strength, and toughness matching between the weld and the base metal is given more consideration (Monsef et al., 2021). Now, the composition and structure of the weld are different from that of the base metal. In fact, for welded structures utilized in environments conducive to stress corrosion, when selecting welding materials, we should consider not only the weldability of base metal but also ensure its service performance, that is, ensuring that no corrosion cracking takes place. This requires that the difference between the chemical and electrochemical properties of the weld and the base metal should not be too great; otherwise, corrosion occurs too readily. In order to improve the corrosion resistance of welded joints, according to the principle of electrochemical corrosion, the same welding materials as the base metal should be used to make the electrochemical properties of the base metal and the weld metal similar to each other. However, it is still difficult to achieve this in practice, and further research is needed on the subject.

5 Conclusion

The corrosion resistance of HSAL weld metal with different alloy compositions was studied in this paper. The corrosion resistance of 460 MPa high-temperature ultra-high strength weld metal, 690 MPa high-temperature ultra-high strength weld metal, and 980 MPa high-temperature ultra-high strength weld metal in an atmospheric environment was studied by both an SKP test and a corrosion weight loss test. At the same time, the corrosion resistance of the 460 MPa high-temperature ultra-high strength weld metal, the 690 MPa high-temperature ultra-high strength weld metal, and the 980 MPa high-temperature ultra-high strength weld metal in simulated seawater was studied by seawater immersion corrosion and electrochemical tests. The main conclusions are as follows:

- 1) The corrosion weight gain of the 980 MPa HSAL weld metal in the atmospheric environment was the smallest, the V A potential the highest, and the corrosion weight loss rate is the

lowest. Compared with 460 MPa HSAL weld metal and 690 MPa HSAL weld metal, it has better corrosion resistance in an atmospheric environment;

- 2) In the simulated seawater environment, the 980 MPa HSAL weld metal had the lowest corrosion and self-corrosion current, showing good corrosion resistance. The corrosion resistance of 690 MPa HSAL was mid-range, and that of 460 MPa HSAL was the lowest. At the same time, among the three HSALs, corrosion resistance of the weld area is primarily attributable to the base metal area, and the corrosion resistance of the heat-affected zone is the worst.

Data availability statement

The raw data supporting the conclusion of this article will be made available by the authors, without undue reservation.

Author contributions

LS: conceptualization and methodology. YP: data curation and writing—original draft preparation. HZ: visualization and

investigation. YC: supervision. QF: writing—reviewing and editing.

Funding

The study was supported by the National Key Research and Development Program of China (Grant No. 2017YFB0304700).

Conflict of interest

The authors declare that the research was conducted in the absence of any commercial or financial relationships that could be construed as a potential conflict of interest.

Publisher's note

All claims expressed in this article are solely those of the authors and do not necessarily represent those of their affiliated organizations, or those of the publisher, the editors, and the reviewers. Any product that may be evaluated in this article, or claim that may be made by its manufacturer, is not guaranteed or endorsed by the publisher.

References

- Ding, S., Xiang, S., Ba, X., Zhang, X., and Fu, Y. (2020). Improvement of corrosion resistance of simulated weld heat affected zone in high strength pipeline steel using electropulsing. *ISIJ Int.* 60 (9), 2015–2023. doi:10.2355/isijinternational.isijint-2019-565
- Garcia, M., and Procópio, L. (2020). Distinct profiles in microbial diversity on carbon steel and different welds in simulated marine microcosm. *Curr. Microbiol.* 77 (6), 967–978. doi:10.1007/s00284-020-01898-4
- Gucwa, M., Winczek, J., Giza, K., Wiecek, P., and Makles, K. (2019). The effect of welding methods on the corrosion resistance of 304 stainless steel joints. *Acta Phys. Pol. A* 135 (2), 232–235. doi:10.12693/aphyspola.135.232
- Jiang, B., Guo, T., Peng, Q., Jiao, Z., Volinsky, A. A., and Gao, L. (2019). Proton irradiation effects on the electron work function, corrosion and hardness of austenitic stainless steel phases. *Corros. Sci.* 157, 498–507. doi:10.1016/j.corsci.2019.06.011
- Kse, C. (2020). Characterization of weld seam surface and corrosion behavior of laser-beam-welded aisi 2205 duplex stainless steel in simulated body fluid. *J. Mat. Sci.* 55 (36), 17232–17254. doi:10.1007/s10853-020-05326-7
- Lanzutti, A., Andreatta, F., Lekka, M., and Fedrizzi, L. (2019). Microstructural and local electrochemical characterisation of gr. 91 steel-welded joints as function of post-weld heat treatments. *Corros. Sci.* 148, 407–417. doi:10.1016/j.corsci.2018.12.042
- Ma, C., Han, E. H., Peng, Q., and Ke, W. (2018). Effect of polishing process on corrosion behavior of 308L stainless steel in high temperature water. *Appl. Surf. Sci.* 442 (1), 423–436. doi:10.1016/j.apsusc.2017.12.190
- Monsef, R., Ghiyasiyan-Arani, M., and Salavati-Niasari, M. (2021). Design of magnetically recyclable ternary Fe₂O₃/EuVO₄/g-C₃N₄ nanocomposites for photocatalytic and electrochemical hydrogen storage. *ACS Appl. Energy Mater.* 4, 680–695. doi:10.1021/acsaem.0c02557
- Ogawa, K., and Osuki, T. (2020). Modelling of sigma phase precipitation in super duplex stainless steel weld metal. *ISIJ Int.* 60 (5), 1016–1021. doi:10.2355/isijinternational.isijint-2019-537
- Radhamani, A. V., Lau, H. C., and Ramakrishna, S. (2020). Nanocomposite coatings on steel for enhancing the corrosion resistance: A review. *J. Compos. Mater.* 54 (5), 681–701. doi:10.1177/0021998319857807
- Sarkar, S., Sarswat, P. K., and Free, M. L. (2018). Metal oxides and novel metallates coated stable engineered steel for corrosion resistance applications. *Appl. Surf. Sci.* 456, 328–341. doi:10.1016/j.apsusc.2018.06.064
- Shen, L., Zhao, W., and Miao, L. (2020). Designed a novel ep + go/zrc + go coating with bilayered structure for enhancing corrosion resistance of steel substrate. *J. Hazard. Mater.* 403 (9), 123670. doi:10.1016/j.jhazmat.2020.123670
- Sinhmar, S., and Dwivedi, D. K. (2018). A study on corrosion behavior of friction stir welded and tungsten inert gas welded aa2014 aluminium alloy. *Corros. Sci.* 133, 25–35. doi:10.1016/j.corsci.2018.01.012
- Song, M. G., Kim, H. K., and Lee, S. Y. (2019). Effect of a zn interlayer on the adhesion strength and corrosion resistance of zn-mg coated trip steel. *ISIJ Int.* 59 (6), 1113–1118. doi:10.2355/isijinternational.isijint-2018-476
- Tomarov, G. V., Shipkov, A. A., and Komissarova, T. N. (2019). Local flow-accelerated corrosion of welds in npp power unit pipelines: Phenomenon mechanism features and measures to prevent damage. *Therm. Eng.* 66 (2), 138–147. doi:10.1134/s0040601519020083
- Wang, K., Wei, A., Tong, X., Lin, J., Jin, L., Zhong, X., et al. (2018). Improvement of the anti-corrosion property of twinning-induced plasticity steel by twin-induced grain boundary engineering - sciencedirect. *Mater. Lett.* 211, 118–121. doi:10.1016/j.matlet.2017.09.102
- Yang, T., Chen, W. L., Gou, G. Q., Tian, H. L., and Chen, Y. (2018). Modeling of corrosion fatigue life of stainless steel joints welded by laser-metal active gas hybrid welding. *CORROSION* 74 (10), 1132–1140. doi:10.5006/2786
- Zhang, H., Xue, P., Wang, D., Wu, L. H., Ni, D. R., and Xiao, B. L. (2019). A novel approach to achieve high yield strength high nitrogen stainless steel with superior ductility and corrosion resistance. *Mater. Lett.* 242, 91–94. doi:10.1016/j.matlet.2019.01.078
- Zhang, J. C., Wang, X. H., Zhang, M., and Zeng, B. (2018). Penetration experiment and simulation of welds based on bulletproof steel plate. *Comput. Simul.* 35 (11), 17–21.
- Zhang, Z., Jing, H., Xu, L., Han, Y., Lei, Z., Lv, X., et al. (2018). Effect of post-weld heat treatment on microstructure evolution and pitting corrosion resistance of electron beam-welded duplex stainless steel. *Corros. Sci.* 141, 30–45. doi:10.1016/j.corsci.2018.06.030